Article

Mechanism of Activity-Dependent Cargo Loading via the Phosphorylation of KIF3A by PKA and CaMKIIa

Highlights

- The cargo-bound KIF3A was phosphorylated by specific kinases, PKA and CaMKIIa

- Phosphorylation of the KIF3A upregulates the loading and transport of N-cadherin

- N-cadherin was accumulating in the spine during homeostatic plasticity

- Phospho-KIF3A enhances the N-cadherin accumulation during homeostatic plasticity

Authors

Sotaro Ichinose, Tadayuki Ogawa, Nobutaka Hirokawa

Correspondence

hirokawa@m.u-tokyo.ac.jp

In Brief

Ichinose et al. identified critical KIF3A phosphorylation sites and specific kinases for a cargo loading. This phosphorylation was elevated during homeostatic plasticity. They propose the first model that the phosphorylation of KIF3A upregulates the cargo loading in an activity-dependent manner.

CrossMark

CellPress

Mechanism of Activity-Dependent Cargo Loading via the Phosphorylation of KIF3A by PKA and CaMKIIa

Sotaro Ichinose,[1] Tadayuki Ogawa,[1] and Nobutaka Hirokawa[1,2,*]
[1]Department of Cell Biology and Anatomy, Graduate School of Medicine, University of Tokyo, Hongo, Bunkyo-ku, Tokyo 113-0033, Japan
[2]Center of Excellence in Genome Medicine Research, King Abdulaziz University, Jeddah 21589, Saudi Arabia
*Correspondence: hirokawa@m.u-tokyo.ac.jp
http://dx.doi.org/10.1016/j.neuron.2015.08.008

SUMMARY

A regulated mechanism of cargo loading is crucial for intracellular transport. N-cadherin, a synaptic adhesion molecule that is critical for neuronal function, must be precisely transported to dendritic spines in response to synaptic activity and plasticity. However, the mechanism of activity-dependent cargo loading remains unclear. To elucidate this mechanism, we investigated the activity-dependent transport of N-cadherin via its transporter, KIF3A. First, by comparing KIF3A-bound cargo vesicles with unbound KIF3A, we identified critical KIF3A phosphorylation sites and specific kinases, PKA and CaMKIIa, using quantitative phosphoanalyses. Next, mutagenesis and kinase inhibitor experiments revealed that N-cadherin transport was enhanced via phosphorylation of the KIF3A C terminus, thereby increasing cargo-loading activity. Furthermore, N-cadherin transport was enhanced during homeostatic upregulation of synaptic strength, triggered by chronic inactivation by TTX. We propose the first model of activity-dependent cargo loading, in which phosphorylation of the KIF3A C terminus upregulates the loading and transport of N-cadherin in homeostatic synaptic plasticity.

INTRODUCTION

Kinesin superfamily proteins (KIFs) are microtubule (MT)-dependent molecular motors that function in intracellular transport. KIFs transport various types of cargo, including organelles, synaptic vesicle precursors, neurotransmitter receptors, cell signaling molecules, cell adhesion molecules, and mRNAs (Hirokawa, 1998; Hirokawa et al., 2010). KIF3, a member of the kinesin-2 family, forms a heterotrimeric complex that consists of KIF3A, KIF3B, and kinesin-associated protein 3 (KAP3) (Kondo et al., 1994; Teng et al., 2005; Yamazaki et al., 1996). KIF3 has been reported to be essential for the intraciliar/intraflagellar transport that is responsible for left/right determination of mammalian embryos (Hirokawa et al., 2009b) and to be impor-

tant for cell polarity establishment (Nishimura et al., 2004) and voltage-gated potassium channel transport (Gu et al., 2006; Gu and Gu, 2010).

In neurons, KIFs manage fundamental neuronal functions such as viability, morphogenesis, and synaptic plasticity (Hirokawa et al., 2010). To achieve these effects, KIFs must be regulated to load their specific cargoes effectively, transport the cargoes along MTs, and release them at precise positions under specific regulatory mechanisms. For example, protein phosphorylation, Rab GTPases, and Ca^{2+} signaling have been reported to contribute to this regulation (Guo et al., 2005; Hill et al., 2000; Hirokawa et al., 2009a; Niwa et al., 2008; Stowers et al., 2002). Recently, protein kinases have been reported to have important roles in the cargo release mechanism. For example, CaMKII, which controls learning and memory activities, phosphorylates KIF17 to trigger the release of its cargo (Guillaud et al., 2008; Yin et al., 2012). By contrast, the cargo loading mechanism remains unknown.

Synaptic plasticity is an important process for learning and memory. Hebbian plasticity, including long-term potentiation (LTP) and long-term depression (LTD), is a well-studied positive feedback system in neurons (Malenka and Bear, 2004). This type of plasticity strengthens individual synaptic input, thus reinforcing specific networks. Homeostatic plasticity such as synaptic scaling has recently been studied as a negative feedback system. This negative feedback system allows neurons to stabilize their firing without changing the relative strength of synaptic inputs such that information stored by changes in synaptic weight induced by LTP and LTD is not disrupted (Turrigiano, 2008). Thus, the combination of Hebbian and homeostatic plasticity seems to sustain proper network activities in higher brain functions such as memory consolidation during sleep (Tononi and Cirelli, 2014).

N-cadherin is one of the calcium-dependent, homophilic cell-cell adhesion molecules important for synaptic plasticity (Brigidi and Bamji, 2011; Takeichi, 2014; Vitureira and Goda, 2013). For example, synthesized N-cadherin is recruited to enlarged spines upon the induction of late-phase LTP (Bozdagi et al., 2000; Mendez et al., 2010). Postsynaptic N-cadherin and β-catenin also control miniature excitatory postsynaptic current (mEPSC) amplitudes in homeostatic synaptic plasticity (Okuda et al., 2007; Vitureira et al., 2012). Therefore, synaptic strength involves the accumulation of N-cadherin at synapses. Our previous
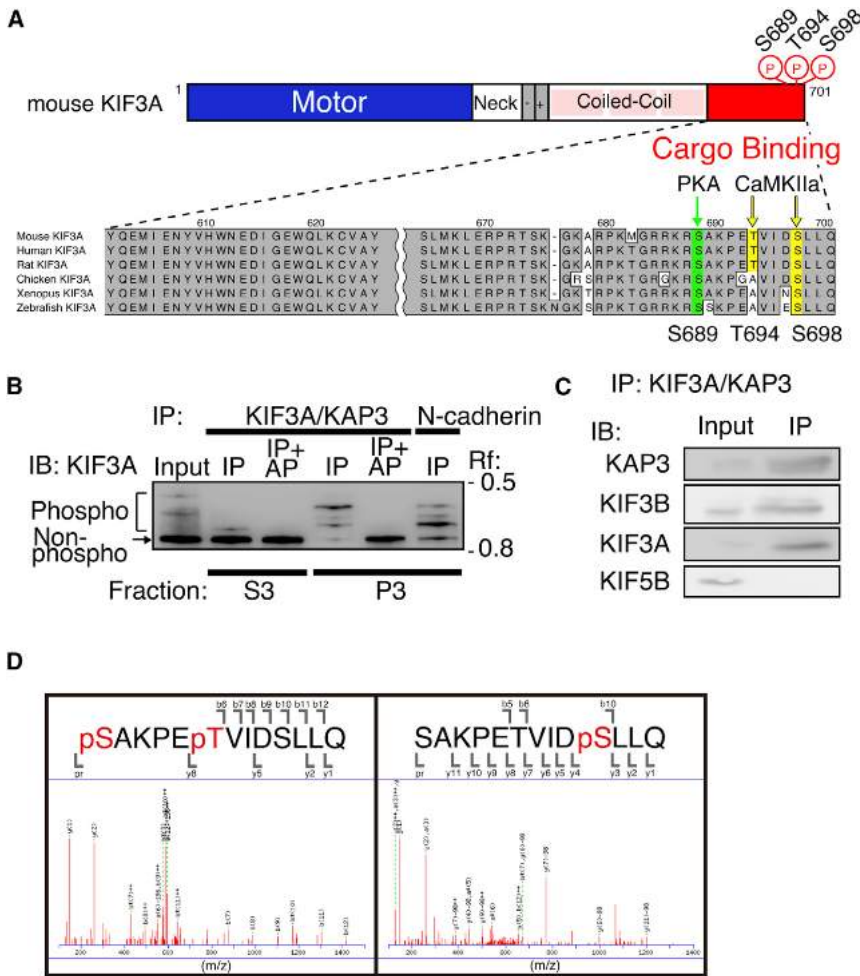
A

S689 T694 S698

mouse KIF3A 1 | Motor | Neck | − + | Coiled-Coil | | 701

Cargo Binding

PKA CaMKIIa

| | 610 | | 670 | | 680 | | 690 | | 700 |
Mouse KIF3A | YQEMIENYVHWNEDIGEWQLKCVAY | SLMKLERPRTSK-GKARPKMGRRKRSAKPETVIDSLLQ |
Human KIF3A | YQEMIENYVHWNEDIGEWQLKCVAY | SLMKLERPRTSK-GKARPKTGRRKRSAKPETVIDSLLQ |
Rat KIF3A | YQEMIENYVHWNEDIGEWQLKCVAY | SLMKLERPRTSK-GKARPKTGRRKRSAKPETVIDSLLQ |
Chicken KIF3A | YQEMIENYVHWNEDIGEWQLKCVAY | SLMKLERPRTSK-GRSRPKTGRGKRSAKPGAVIDSLLQ |
Xenopus KIF3A | YQEMIENYVHWNEDIGEWQLKCVAY | SLMKLERPRTSK-GKTRPKTGRRKRSAKPFAVINSLLQ |
Zebrafish KIF3A | YQEMIENYVHWNEDIGEWQLKCVAY | SLMKLERPRTSKNGKSRPKTGRRKRSKPEAVIESLLQ |

S689 T694 S698

B

IP: KIF3A/KAP3 N-cadherin

IB: KIF3A   Input IP   IP+AP IP IP+AP IP   Rf:
− 0.5
Phospho
Non-phospho
− 0.8

Fraction: S3   P3

C IP: KIF3A/KAP3

IB: Input IP
KAP3
KIF3B
KIF3A
KIF5B

D

b6 b7 b8 b9 b10 b11 b12
pSAKPEpTVIDSLLQ
y8 y5 y2 y1

b5 b6 b10
SAKPETVIDpSLLQ
y11 y10 y9 y8 y7 y6 y5 y4 y3 y2 y1

(m/z)   (m/z)

Figure 1. KIF3A Is Phosphorylated at S689, T694, and S698 In Vivo

(A) Summary of the phosphorylation sites of mouse KIF3A in vivo and in vitro. The C-terminal amino acid sequences corresponding to the cargo-binding site in the KIF3A domain are aligned within the KIF3 family. S689 is phosphorylated by PKA (green); T694 and S698 are phosphorylated by CaMKIIa (yellow). − and + represent charged regions. "P" (red) indicates phosphorylation.

(B) Phosphorylation of fractionated KIF3A from whole brain. S3 (S3-KIF3A) and P3 fractions (P3-KIF3A) were immunoprecipitated (IP) with anti-KIF3A/KAP3 and anti-N-cadherin antibodies from each fraction. P3-KIF3A shows multiple phosphorylation patterns by Phos-tag SDS-PAGE. The shifted bands disappeared upon alkaline phosphatase (AP) treatment. Rf stands for relative migration distance.

(C) Purification of native KIF3 complex from whole brain. IP samples were separated on conventional SDS-PAGE and immunoblotted with KIF3/KAP3 antibodies.

(D) Typical MS/MS spectrum of the phosphorylated peptides of KIF3A from brain. The KIF3A peptides (aa 689–701) pSAKPEpTVIDSLLQ and SAKPETVIDpSLLQ are shown.

See also Figure S1.

work showed that N-cadherin was transported by KIF3 (Teng et al., 2005). This evidence suggests the testable model that N-cadherin loading and transport via KIF3 may be controlled by the upregulation of synaptic strength.

Here, we show that activity-dependent phosphorylation of KIF3A facilitates N-cadherin loading and transport. First, by comparing KIF3A bound to cargo vesicles with unbound KIF3A, we determine the phosphorylation sites and responsible kinases for each site, which could regulate cargo loading, using quantitative proteomic approaches. We demonstrate that KIF3A S689 was phosphorylated by PKA and that T694 and S698 were phosphorylated by CaMKIIa both in vitro and in vivo. Both PKA and CaMKII are known to be important kinases in synaptic plasticity (Banke et al., 2000; Bemben et al., 2014; Diering et al., 2014; Esteban et al., 2003; Frey et al., 1993; Hell, 2014; Hoerndli et al., 2015; Opazo et al., 2010; Roche et al., 1996). Next, we show that the phosphorylation within the KIF3A cargo-binding site increased the affinity between KIF3A and N-cadherin, resulting in the enhancement of N-cadherin transport and spine enlargement. Interestingly, when neuronal activity was chronically suppressed by tetrodotoxin (TTX), the levels of N-cadherin expression and KIF3A phosphorylation were elevated. Simultaneously, the transport of

N-cadherin was enhanced; this enhancement resulted in global spine enlargement. Taking these results together, we hereby propose a model of the activity-dependent cargo loading and transport mechanism: the phosphorylation of the KIF3A C terminus upregulates the loading and transport of N-cadherin. This mechanism may have an important role in synaptic function and plasticity.

RESULTS

Cargo-Bound KIF3A Is Highly Phosphorylated In Vivo

Molecular motors are known to display two functionally different distributions: cytosolic states free from cargo binding and particulate states bound to cargoes, vesicles, or membranes. Thus, we hypothesized that KIF3 and its cargo might be functionally regulated by specific kinase signaling pathways. To elucidate the functional significance of KIF3A phosphorylation, we first compared the phosphorylation level of free KIF3A in the cytosolic fraction (S3-KIF3) with that of cargo-bound KIF3 in the particulate fraction (P3-KIF3) from mouse brain by Phos-tag western blot (WB) using antibodies against KIF3A and KAP3. In contrast to S3-KIF3, P3-KIF3 displayed apparent band shifts caused by KIF3A phosphorylation (Figure 1B). These band shifts disappeared upon alkaline phosphatase (AP) treatment, confirming that the band shifts definitely reflect KIF3A phosphorylation. In addition, KIF3A that coimmunoprecipitated with anti-N-cadherin showed substantial phosphorylated band shifts that were nearly equal to that of KIF3A purified with anti-KIF3A

and anti-KAP3 (Figure 1B). These results indicate that cargo-bound KIF3A is highly phosphorylated compared with free KIF3A and that KIF3A phosphorylation is functionally significant in vivo.

The Cargo-Binding Domain of KIF3A-tail Is Multiply Phosphorylated In Vivo

Given the finding that phosphorylation might be an important cue in cargo-bound KIF3A compared with free KIF3A, we further examined KIF3A phosphorylation. Native KIF3A was immunoprecipitated from the mouse brain S2 fraction. KIF3B/C/KAP3, components of the KIF3/KAP3 complex, were also successfully copurified and identified by western blot and MALDI-TOF/TOF mass spectrometry (Figure 1C and see Figure S1A available online). Trypsinized KIF3A peptides were separated on tandem affinity columns for phosphopeptides, and eluted peptides were analyzed on an LC-MS/MS system. Through these analyses, we obtained sufficient sequence coverage (61%) for phosphoanalysis of KIF3A and identified S689, T694, and S698 as phosphorylation sites in vivo (Figures 1A, 1D, S1B, and S1C). Interestingly, these phosphorylation sites were conserved and located on the C terminus of KIF3A, which is known as a cargo-binding site critical for cargo transport activity; hence, phosphorylation of this domain appears to be functionally important for cargo loading and transport via KIF3A in the brain.

PKA and CaMKIIa Specifically Phosphorylate the C Terminus of KIF3A In Vitro

Protein phosphorylation occurs downstream of specific signaling cascades in vivo. To reveal the specific signaling to KIF3A, we first sought to identify the specific kinases that phosphorylate KIF3A by in vitro kinase assay. Bacterially expressed KIF3A C terminus protein (GST–KIF3ACT in Figure S2) was assayed with 40 active kinases in vitro. Phos-tag SDS-PAGE showed phosphorylation-dependent band shifts driven by 17 kinases, AKT1, AKT2, CaMKIIa, CaMKIV, CK2, DYRK1B, IKKb, MAPK11/p38β, MAPK12/p38γ, MAPK14/p38α, MARK1, MARK2, PAK1, PKA, PKCα, PKCδ, and RSK1, indicating that these were candidate kinases for KIF3A C-terminal phosphorylation. Among these candidates, we focused on five kinases, CaMKIIa, CaMKIIb, PKA, PKCα, and RSK1, based on their target motifs and functions in neurons.

To identify the kinases responsible for the phosphorylation of S689, T694, and S698 under physiological conditions, kinase assay samples were further analyzed by a quantitative proteomic approach using LC-MS/MS with tandem mass tag (TMT) labeling. Although three possible phosphorylation sites were located within the peptide, KIF3A C terminus phosphopeptides were successfully separated into two populations, pSAKPETVIDSLLQ and SAKPEpTVIDSLLQ/SAKPETVIDpSLLQ, on the nano-LC system (retention time, 8.4 and 19 min, respectively; Figure 2B). In addition, quantitation of the intensities of the reporter ions from TMT-tag revealed that PKA preferentially phosphorylated S689 (Figure 2B, upper), whereas CaMKIIa phosphorylated T694 and S698 (Figure 2B, lower). Interestingly, S689 is part of the consensus sequence for both PKA and CaMKs (RXXS/T); however, this site was only phosphorylated by PKA. Instead, CaMKIIa phosphorylated T694 or S698, which are not part of

any consensus sequences. This quantitative approach excluded false-positive identification, biased prejudice from consensus sequence, and experimental error.

To confirm this phosphorylation by PKA and CaMKIIa in vitro, bacterially expressed GST–KIF3ACT WT and unphosphorylatable mutant GST–KIF3ACT AAA (S689A/T694A/S698A) were assayed with CaMKIIa, PKA, and PKCα. As expected, GST–KIF3ACT AAA incubated with CaMKIIa or PKA showed markedly reduced phosphorylation compared with GST–KIF3ACT WT, while GST–KIF3ACT AAA incubated with PKCα displayed the same phosphorylation level as WT (Figure 2C). Taken together, PKA and CaMKIIa specifically phosphorylated the three residues in the cargo-binding site of the KIF3A C terminus.

KIF3A Phosphorylation Occurs Downstream of PKA/CaMKIIa Activation In Vivo

We identified PKA and CaMKIIa as the kinases responsible for the phosphorylation of KIF3A S689/T694/S698 within the cargo-binding sites in vitro. To test whether endogenous KIF3A was actually phosphorylated downstream of PKA and CaMKIIa in vivo, cultured cortical neurons grown for 14 days in vitro (DIV 14) were treated with the following inhibitors or stimulators of PKA and CaMK: KT5720, which inhibits PKA; KN-93, which inhibits CaMKII; forskolin (FSK), which activates PKA; and thapsigargin (ThG), which activates CaMKII by inhibiting endoplasmic reticulum calcium ATPase. The phosphorylation level of KIF3A was increased in FSK- or ThG-stimulated neurons; in addition, inhibition of PKA and CaMKII by KT5720 and KN-93 did not affect KIF3A phosphorylation (Figure 2D). To confirm site-specific phosphorylation under physiological conditions, mouse cortical neurons transfected with GFP–KIF3A WT or the GFP–KIF3A AAA mutant with and without stimulation were analyzed by Phos-tag WB. Phosphorylation-dependent multiple band shifts were directly observed only in GFP–KIF3A WT under PKA/CaMKIIa stimulation (Figure 2E). These data confirm that S689, T694, and S698 of the KIF3A C terminus were phosphorylated downstream of PKA/CaMKIIa in vivo.

Phosphorylation of S689/T694/S698 Enhances the Cargo-Binding Activity of KIF3A

As previously reported, the KIF3/KAP3 complex transports N-cadherin (Teng et al., 2005). Because P3-KIF3A is definitely phosphorylated more than S3-KIF3A and because the phosphorylation sites are localized in the C-terminal cargo-binding site of KIF3A, we investigated how phosphorylation directly affects the function of the KIF3A. We focused on two major functions of the tail regions of KIFs: the binding activity with cargoes and motility regulation through an autoinhibition system (Hirokawa et al., 2010).

We first investigated the binding activity of KIF3A mutants with N-cadherin complexes under physiological conditions. The result of the GST pull-down assay using brain lysate indicated that approximately twice as many β-catenin/N-cadherin complexes were pulled down with the phosphomimetic mutant (GST–KIF3ACT EEE: S689E/T694E/S698E) compared with the unphosphorylatable mutant (GST–KIF3ACT AAA: S689A/T694A/S698A) (Figures 3A and 3B). Moreover, this result suggests that KIF3A phosphorylation on S689/T694/S698 increased
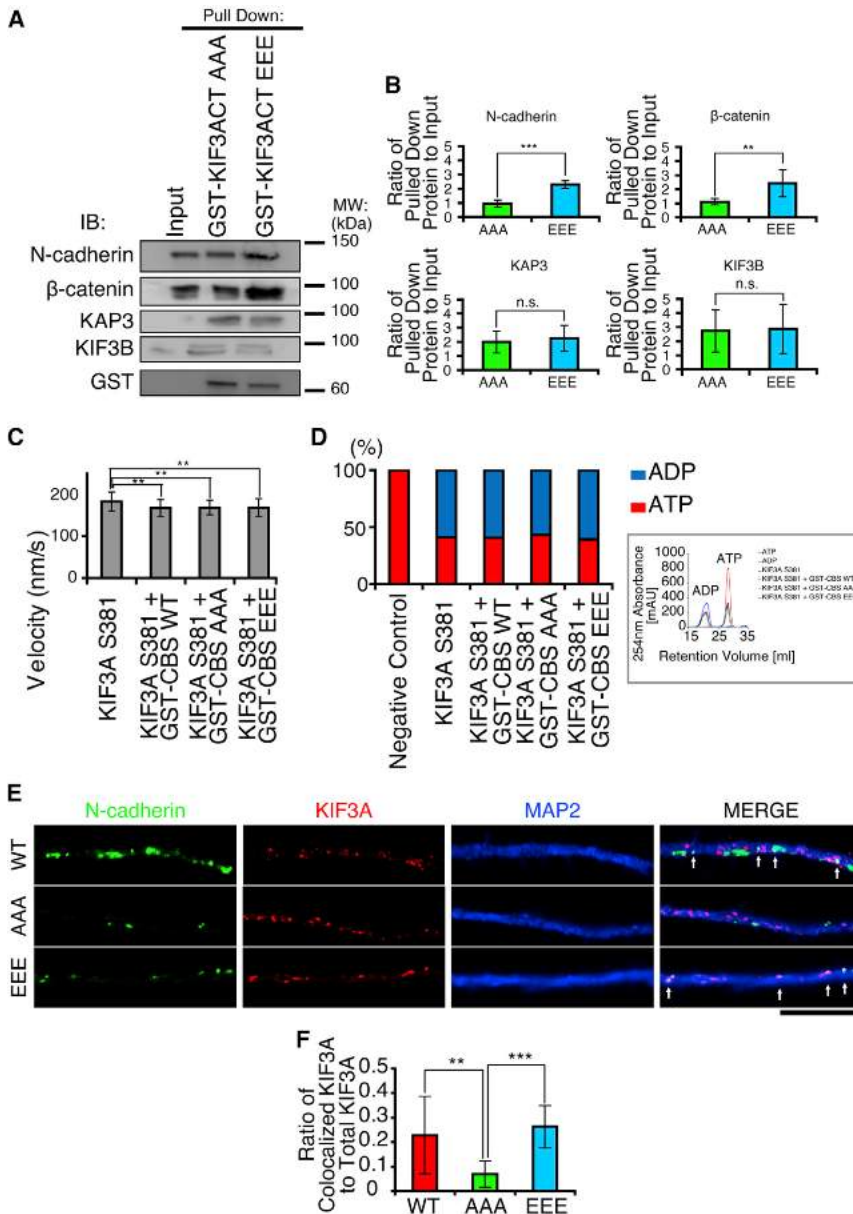
Figure 2. PKA Phosphorylated S689, and CaMKIIa Phosphorylated T694 and S698

(A) Kinase assay samples developed by Phos-tag SDS-PAGE. GST–KIF3ACT was assayed with serine/threonine kinases in vitro. NC represents negative control incubated without kinase. Phosphorylation was detected as upwardly shifted bands (red arrowheads).

(B) Quantitation of phosphopeptides in two different chromatogram extractions. The peptide pSAKPETVIDSLLQ, retained for 8.4 min on LC, was preferentially phosphorylated by PKA. The peptides SAKPEpTVIDSLLQ/SAKPETVIDpSLLQ, retained for 19 min on LC, were phosphorylated at T694 or S698 by CaMKIIa. The phosphorylation of the same samples was also confirmed by Phos-tag WB (Figure S3).

(C) Phosphorylation of GST–KIF3ACT mutants in vitro. GST– KIF3ACT mutants (wild-type or mutant) were assayed with CaMKIIa, PKA, and PKCa (1 hr). Phospho-GST–KIF3ACT WT was detected as bands that migrated higher. CaMKIIa and PKA phosphorylated GST–KIF3ACT AAA (S689A/T694A/S698A) less than did WT. Rf stands for relative migration distance.

(D) Phosphorylation of native KIF3A in stimulated neurons. Cortical neurons were stimulated with inhibitors, forskolin, or thapsigargin. Cortical cultured neurons grown for 14 days in vitro (DIV 14) were treated with the PKA inhibitor KT5720, the CaMKII inhibitor KN-93 (1 hr), the PKA activator forskolin (20 min), or thapsigargin, which induces ER calcium release and thereby activates CaMKII (30 min). Phospho-KIF3A is detected as the upper bands (asterisk). FSK represents forskolin, and ThG represents thapsigargin. Rf stands for relative migration distance.

(E) Phosphorylation of GFP–KIF3A in stimulated cortical neurons. Cortical neurons expressing GFP–KIF3A (wild-type or mutants) were treated with both forskolin and thapsigargin (30 min). Phospho-KIF3A is detected as the upper bands (asterisk). The number and relative intensity of the upper bands decreased in KIF3A AAA treated with forskolin and thapsigargin compared with KIF3A WT. Rf stands for relative migration distance.

the affinity of KIF3A for the vesicles containing N-cadherin. Interestingly, no significant difference in the amounts of KAP3 and KIF3B was observed between these mutants, indicating that this phosphorylation would not affect the interactions within the KIF3/KAP3 heterotrimer (Figures 3A and 3B).

We next examined the effects of C-terminal phosphorylation on motor activity. Some KIFs are reported to be regulated through an autoinhibition system with their own tail region (Dietrich et al., 2008; Imanishi et al., 2006); however, autoinhibition of KIF3 has not yet been reported. Therefore, to investigate the direct effects of C-terminal phosphorylation on KIF3A motor activity, the MT gliding velocity and the MT-stimulated ATPase activity were measured in the presence of KIF3-tail mutants in vitro (Figures 3C and 3D). The KIF3A motor (KIF3A S381) showed approximately 170 nm/s velocities of MT gliding in the presence of the KIF3A-tail GST–CBS WT and mutants GST–CBS AAA and GST–CBS EEE compared to that without the tail region (180 nm/s velocity). These slightly different velocities between the KIF3 motors with/without the tail region might reflect the existence of a weak KIF3A autoinhibition system. However, no significant difference was observed between mutants (Figure 3C), indicating that phosphorylation on this tail region does not directly contribute to motor activity regulation. The MT-activated ATPase activity in the presence of the tail mutants also displayed no significant difference between mutants (Figure 3D). Taken together, these results indicate that phosphorylation of

Figure 3. Phosphorylation of KIF3A at S689, T694, and S698 Affects Cargo-Binding Activity

(A) Phosphorylation increases the affinity between KIF3A and its cargo. GST pull-down assays were performed using unphosphorylatable GST–KIF3ACT AAA or phosphomimetic GST–KIF3ACT EEE from the brain S2 fraction. Immunoblots show N-cadherin, β-catenin, KAP3, KIF3B, and GST. MW stands for molecular weight.

(B) Quantification of GST pull-down assays (n = 6). Ratios of pulled down proteins were normalized to the signals of GST. GST–KIF3ACT EEE showed increased affinity with cargoes. No significant change in affinity was observed between KIF3 components (p > 0.05). Histograms, mean ± SD, **p < 0.01, ***p < 0.001; n.s., not significant, t test.

(C) MT gliding assays. MT velocities in the presence of 10 mM cargo-binding site (wild-type or mutants) are shown. KIF3A motor: 183.6 ± 22.4 nm/s; KIF3A motor + GST-CBS WT: 168.1 ± 20.1 nm/s; KIF3A motor + GST-CBS AAA: 169.0 ± 17.5 nm/s; KIF3A motor + GST-CBS EEE: 169.1 ± 21.1 nm/s. Histograms, mean ± SD, **p < 0.01, t test, n = 50 from at least 5 independent experiments.

(D) ATPase activity. Ratios of released ADP and bound ATP are shown at 30 min after the reaction of 100 nmol ATP and KIF3A motor in the presence of polymerized MTs and KIF3A C-terminal mutants.

(E) Colocalization of KIF3A mutants with N-cadherin in neurons. Hippocampal neurons (DIV 5) transfected with N-cadherin–GFP and tagRFP–KIF3A (wild-type or mutants) were fixed after treatment with AMP-PNP and saponin. AAA showed decreased colocalization compared with WT and EEE (arrowhead). Scale bar, 20 μm.

(F) Ratio of KIF3A colocalized with N-cadherin to total KIF3A (n = 8 neurons). The colocalization decreased in AAA compared with WT and EEE. Histograms, mean ± SD, **p < 0.01, ***p < 0.001, one-way analysis of variance (ANOVA), Scheffé's post hoc test.

the KIF3A tail region does not directly affect the motor activity but increases the cargo-binding activity of KIF3A for the vesicles containing N-cadherin.

To confirm the increased affinity between phospho-KIF3A and N-cadherin in vivo, we observed the localization of tagRFP–KIF3A mutants and N-cadherin–GFP in hippocampal neurons. Cultured neurons were permeabilized with saponin before fixation to reduce the background signal from diffusing molecules. Direct visualization of tagRFP–KIF3A EEE showed increased colocalization with N-cadherin–GFP in dendritic shafts, whereas tagRFP–KIF3A AAA was distributed in dendrites lacking N-cadherin–GFP (Figures 3E and 3F). This finding indicates that phosphorylated KIF3A on S689/T694/S698 in the cargo-binding site produced higher binding activity with the N-cadherin complex.

Phosphorylation of the KIF3A C Terminus Sustains Synaptogenesis via Enhanced N-Cadherin Loading and Transport

The next question for consideration was how the change in cargo-binding activity affects N-cadherin transport and neuronal function. A previous report showed that N-cadherin localization at synapses is proportional to synapse maturation (Benson and Tanaka, 1998). Together with the above-described results, we hypothesized that the phosphorylation of the KIF3A C terminus during synaptogenesis increases the loading efficiency, thus enhancing N-cadherin transport to the synapses.

To evaluate this hypothesis, cultured hippocampal neurons were transfected with GFP–KIF3A WT, the unphosphorylatable mutant (GFP–KIF3A AAA), or a phosphomimetic mutant (GFP–KIF3A EEE) together with tagRFP. First, we confirmed

Figure 4. Phosphorylation of KIF3A at S689, T694, and S698 Affects Synapse Formation and N-Cadherin Localization

(A) Hippocampal neurons (DIV 12) coexpressing GFP–KIF3A (wild-type or mutants) and tagRFP as a morphological marker. Neurons transfected with KIF3A EEE show large, mushroom-like spines (red arrowhead). Scale bars, 20 μm (top) and 5 μm (bottom).

(B) Quantification of the spine shape, width, length, and area (n = 6 neurons, 240 spines). (a) KIF3A AAA induces filopodia-like thin spines, and KIF3A EEE induces large, mushroom-like spines. (b and c) The spine width of neurons expressing KIF3A EEE differed significantly from that of KIF3A AAA. Histograms depict the spine width (mean ± SEM, ***p < 0.001, one-way ANOVA, Scheffé's post hoc test). Cumulative frequency plots show the spine width (p < 0.001, Kolmogorov-Smirnov (KS) test). (d and e) The spine length of neurons expressing KIF3A EEE did not differ from that of neurons expressing KIF3A AAA. Histograms depict the spine length (mean ± SEM, p > 0.05, one-way ANOVA, Scheffé's post hoc test). Cumulative frequency plots for the spine length (p > 0.05, KS test). (f) Cumulative frequency of the spine area. Neurons expressing KIF3A EEE showed spine areas that differed significantly from that of neurons expressing KIF3A AAA (p < 0.001, KS test).

(C) Hippocampal neurons (DIV 12) coexpressing N-cadherin–GFP and tagRFP–KIF3A (wild-type or mutants). N-cadherin–GFP in the neurons expressing KIF3A EEE had greater accumulation levels at spines than in the neurons expressing KIF3A AAA. Scale bars, 50 μm (left) and 5 μm (right).

(D) The ratio of N-cadherin-positive spines (n = 5 neurons, AAA, 141 spines; EEE, 166 spines). Histograms, mean ± SEM, ***p < 0.001, t test.

that overexpression of GFP-KIF3A WT and RFP did not affect the spine morphologies compared to the neurons expressing only RFP (data not shown). Interestingly, GFP–KIF3A EEE significantly enhanced synapse formation, resulting in large, mushroom-shaped spines more than 1.5 μm in width (Figures 4A and 4B). By contrast, neurons transfected with GFP–KIF3A AAA displayed filopodia-like protrusions on dendritic shafts with high frequency (Figures 4A and 4B). Compared with WT neurons, neurons transfected with the AAA mutant showed no significant differences in spine length. Instead, the width and the area of spine heads were significantly decreased in neurons expressing the AAA mutant (Figures 4A and 4B). These results show that the phosphorylation of the KIF3A C terminus is critical for the enlargement of spines during synaptogenesis.

We next evaluated whether the enlargement of spines is caused by N-cadherin transport using the KIF3A mutants. After cultured hippocampal neurons were transfected with N-cadherin–GFP and tagRFP–KIF3A mutants, N-cadherin localization and accumulation were observed. In neurons transfected with tagRFP–KIF3A EEE, N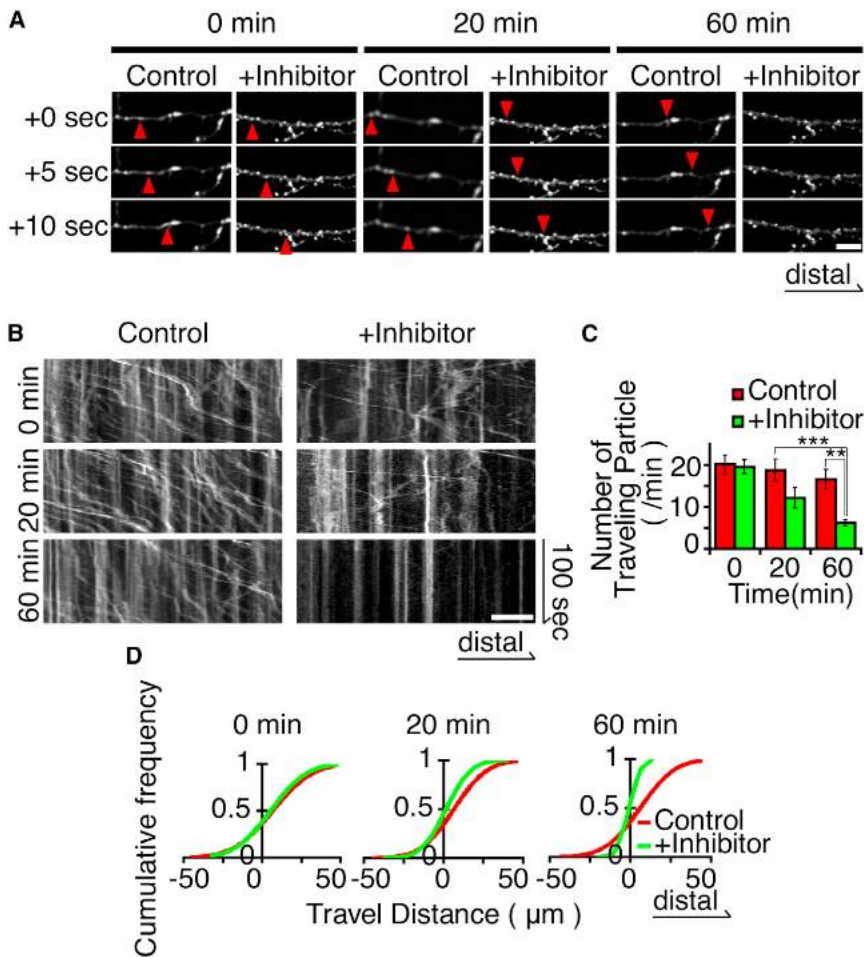-cadherin localized in both spine heads and dendritic shafts, indicating that KIF3A EEE successfully transported N-cadherin into spines. By contrast, in neurons transfected with tagRFP–KIF3A AAA, N-cadherin was retained around the cell body, indicating that KIF3A AAA failed to transport N-cadherin (Figures 4C and 4D). This finding is consistent with the biochemical results that KIF3A EEE showed higher affinity with the N-cadherin complex than did KIF3A AAA (Figures 3A and 3B). These data suggest that phosphorylation of S689/T694/S698 at the KIF3A C terminus enhanced N-cadherin loading and transport, resulting in the enlargement of spines.

PKA and CaMKII Facilitate N-Cadherin Transport in Neurons

To clearly define the N-cadherin transport facilitated downstream of PKA/CaMKIIa, we conducted live imaging and kymograph analyses of N-cadherin while inhibiting PKA/CaMKIIa. Hippocampal neurons were transfected with N-cadherin–GFP, allowing

Figure 5. Kinase Inhibitors Impair the Distal Transport of N-Cadherin

(A) Sequential records of representative N-cadherin transported distally. Hippocampal neurons (DIV 12) were transfected with N-cadherin–GFP and treated with 0.01% DMSO as control or with inhibitors (KT5720, KN-93). Treatment with inhibitors for 60 min prevented N-cadherin transport. Scale bar, 10 μm.

(B) Kymographs of N-cadherin–GFP transport. Treatment with inhibitors gradually reduced the number of N-cadherin–GFP puncta transported distally, which is shown as lines sloping downward to the right. Scale bar, 10 μm.

(C) Numbers of N-cadherin–GFP particles traveling distally per dendrite per minute. Treatment with inhibitors for 60 min significantly decreased the number of traveling particles. Histograms, mean ± SEM, **$p < 0.01$, ***$p < 0.001$, two-way repeated-measures ANOVA, Bonferroni's post hoc test ($n = 8$ dendrites from 4 neurons).

(D) Cumulative frequency of traveling distance of each particle per minute. The treatment with inhibitors did not affect the distance at 0 min ($p > 0.05$) but did affect the distances at 20 min ($p < 0.05$) and 60 min ($p < 0.01$) compared with control. KS test.

precise analysis of distal and proximal movements of N-cadherin in dendrites. Before inhibition, N-cadherin–GFP particles showed bidirectional (distal and proximal) movements along the dendritic shaft; in particular, distal movements were predominant (Figures 5A, 5B, and 5D). At 20 min after the inhibition of PKA/CaMKIIa with KT5720 and KN-93, the number of transported N-cadherin particles in the same dendrite shafts decreased significantly compared with the negative controls (Figures 5A and 5B). Interestingly, this inhibition decreased the distal travel distance but did not affect the proximal travel distance. Further inhibition (60 min) almost abolished the transport of N-cadherin in both directions (Figures 5B–5D). These results are consistent with our results demonstrating that the PKA/CaMKIIa-resistant unphosphorylatable KIF3A (GFP–KIF3A AAA) has less affinity with N-cadherin and could not transport N-cadherin to spines (Figures 3 and 4). Taken together, these observations demonstrate that PKA and CaMKIIa facilitate N-cadherin loading and transport via phosphorylation of S689/T694/S698 in the KIF3A C terminus.

N-Cadherin Is Transported via KIF3A and Accumulated at Spines in Response to Chronic Inactivation

During synapse maturation, N-cadherin is recruited to synaptic sites, and this recruitment is required for synaptic strength and potentiation. Recent reports have shown that chronic inactiva-

tion in immature neurons induced synaptic scaling through the recruitment of AMPAR and adhesion proteins into the spines (Lee et al., 2013; Vitureira and Goda, 2013). Another report showed that N-cadherin has an important role in activity-mediated spine stabilization (Mendez et al., 2010). Thus, we next focused on the facilitation of N-cadherin loading and transport under chronic inactivation evoked by TTX.

To investigate whether the synaptic scaling caused by chronic inactivation correlates with N-cadherin loading and its transport into spines, we observed and quantified both N-cadherin transport and accumulation in dissociated hippocampal neurons under chronic inactivation using TTX. In combination with PKA/CaMKIIa inhibitors, time-lapse imaging showed that the number of enlarged, mature spines containing N-cadherin increased 3 hr after TTX treatment at proximal dendrites (Figures 6A–6C). Immunofluorescence of intrinsic N-cadherin and GluR2/3 displayed nearly identical results (Figure S4). At distal dendrites, N-cadherin increased 12 hr after TTX treatment. This effect of TTX was canceled by the simultaneous addition of the kinase inhibitors KT 5720 and KN-93. These results indicate that chronic inactivation and its downstream kinase signaling cascade enhanced N-cadherin accumulation in spines, thus causing global spine enlargement.

To reveal whether this enhanced accumulation of N-cadherin is driven by the facilitation of N-cadherin transport, we further conducted time-lapse imaging analysis of N-cadherin–GFP in neurons under TTX treatment with/without PKA/CaMKIIa inhibitors. The kymograph analysis showed that the number of N-cadherin particles that traveled distally increased 2-fold compared
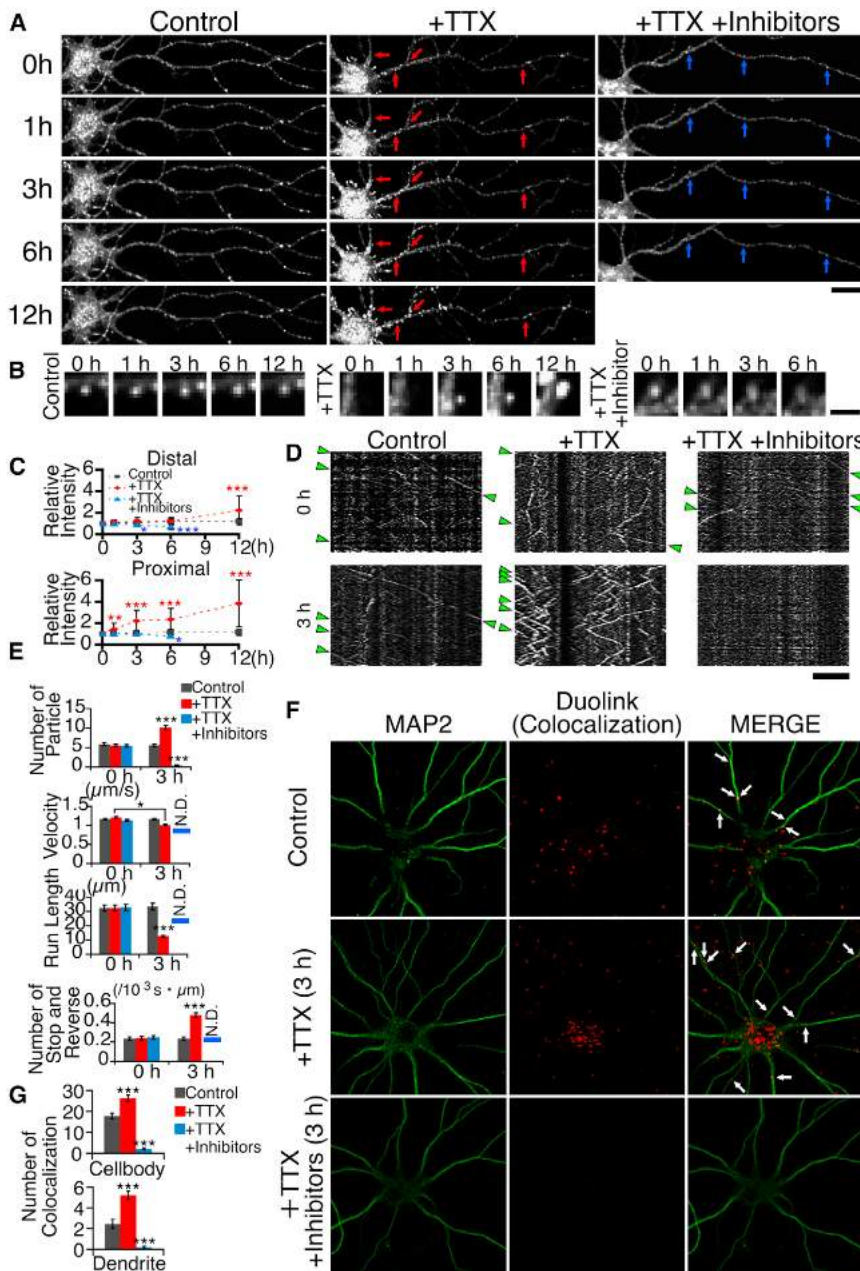
Figure 6. TTX Enhances N-Cadherin Transport and Accumulation

(A) Time-lapse imaging of hippocampal neurons with or without TTX. Hippocampal neurons (DIV 12) were treated with 0.01% DMSO as a control or with TTX, TTX + inhibitor (KT5720 + KN-93) for 12 hr. Neurons treated with TTX and inhibitor generally became unhealthy 12 hr after TTX treatment. Red arrows indicate representative accumulation of N-cadherin. Blue arrows indicate representative reduction of N-cadherin. Scale bar, 20 μm. Immunofluorescence of intrinsic N-cadherin.

(B) Time-lapse imaging of accumulating N-cadherin at spines, high magnification of (A). Neurons treated with TTX showed N-cadherin accumulation, while neurons treated with both TTX and inhibitor showed N-cadherin reduction. Scale bar, 2 μm.

(C) Changes in intensity of N-cadherin clusters (n = 5 neurons). Treatment with TTX for more than 3 hr showed significantly increased intensity in the proximal dendrite, while treatment with TTX for more than 12 hr showed significantly increased intensity in the distal dendrite. Line chart, mean ± SEM, *p < 0.05, **p < 0.01, ***p < 0.001, two-way repeated-measures ANOVA, Scheffé's post hoc test. See also Figure S4.

(D) Kymographs of N-cadherin–GFP transport in neurons. Hippocampal neurons (DIV 12) were transfected with N-cadherin–GFP and treated with 0.01% DMSO (control) or with TTX, or with TTX and inhibitor. To reduce the background noise, acquired live images were processed by the sub-tract function using the ImageJ image calculator, and the signals of N-cadherin movement were extracted. Kymographs show distally directed particles (green) and proximally directed particles. Scale bar, 20 μm.

(E) Statics of distally directed particles in (D; n = 5 neurons). Run length and velocity were not detected (N.D.) in dendrites 3 hr after TTX stimulation with inhibitors. Histograms, mean ± SEM, *p < 0.05, ***p < 0.001, two-way repeated-measures ANOVA, Scheffé's post hoc test.

(F) The proximity ligation assay (Duolink). Duolink assay using anti-KIF3A and anti-N-cadherin antibodies revealed that the colocalization of endogenous KIF3A and N-cadherin increased in both the cell body and the dendritic shafts 3 hr after TTX treatment.

(G) Statics of colocalization between endogenous KIF3A and N-cadherin in (F; n = 30 neurons). Histograms, mean ± SEM, ***p < 0.001, one-way ANOVA, Scheffé's post hoc test.

to that in untreated neurons (Figures 6D and 6E). Interestingly, under TTX stimulation, N-cadherin transport was induced in both directions, with increased numbers of "stop" and "reverse" movements. These effects were suppressed by PKA/CaMKIIa inhibitors. Furthermore, to visualize the interaction between endogenous KIF3A and N-cadherin in neurons, proximity ligation assay (Duolink assay) using anti-KIF3A and anti-N-cadherin antibodies was conducted. Duolink assay revealed that the interaction between endogenous KIF3A and N-cadherin increased in both the cell body and the dendritic shafts following TTX treatment (Figures 6F and 6G). These results indicate that N-cadherin transport via KIF3 was increased by the TTX treatment and decreased by inhibitor treatments. Together with the previous observation of N-cadherin accumulation at spines (Figures 6A and 6D), chronic inactivation with TTX was shown to facilitate N-cadherin transport via KIF3 and induce N-cadherin accumulation at spines, thus resulting in spine enlargement.

Activity-Dependent Phosphorylation of KIF3A Facilitates N-Cadherin Transport

How is N-cadherin transport controlled during chronic inactivation? We have shown that the phosphorylation of the KIF3A
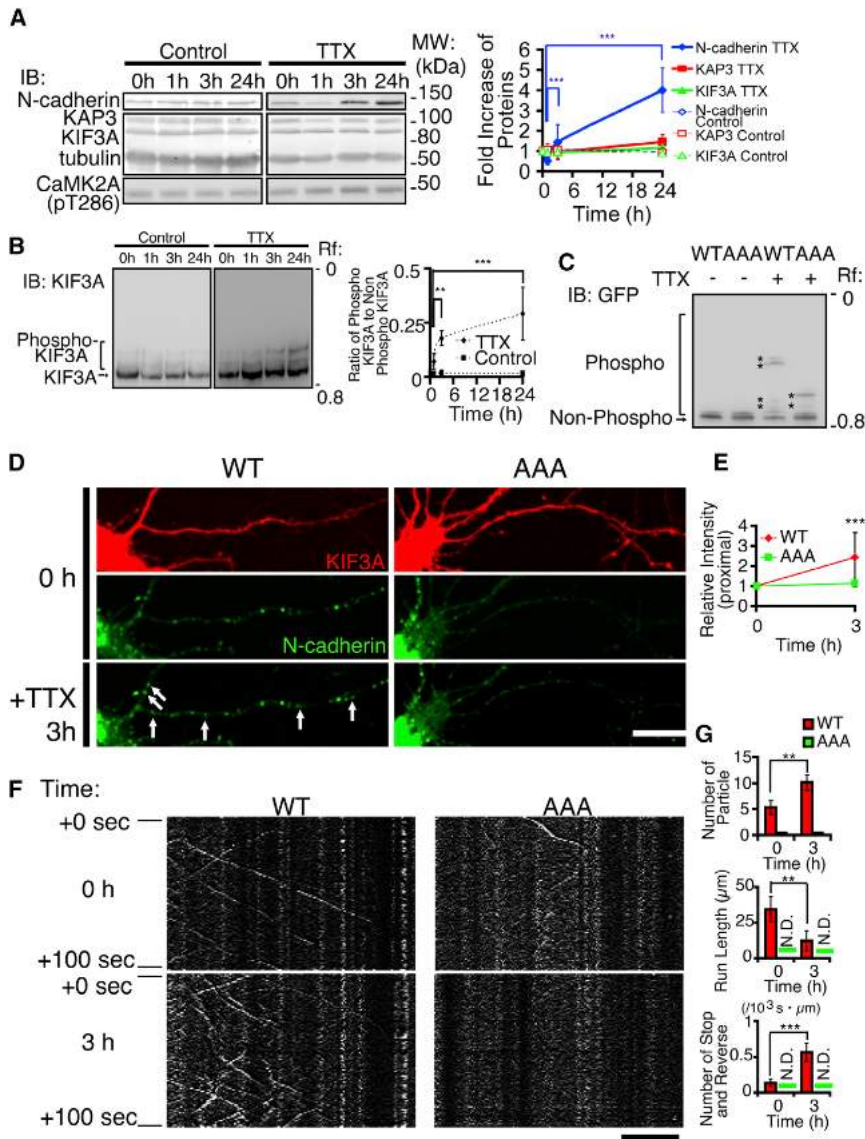
Figure 7. TTX Triggers Phosphorylation of KIF3A at Cargo-Binding Sites

(A) Protein expression levels after TTX treatment. (Left) Cortical neurons (DIV 12) were treated with 0.01% DMSO (control) or TTX and immunoblotted for N-cadherin, KAP3, KIF3A, DM1A (α-tubulin), and CaMKII (pT286) after standard SDS-PAGE. (Right) The fold increases (±SD, n = 4) in proteins relative to 0 hr after treatment, normalized to tubulin. The amounts of KIF3A and KAP3 barely changed with bath application of TTX. The amount of N-cadherin was initially reduced for 1 hr after TTX stimulation but increased beyond the starting level over the next several hours. ***p < 0.001, Dunnett's test.

(B) Increase in KIF3A phosphorylation after TTX stimulation. (Left) Phos-tag WB immunoblotted with anti-KIF3A Ab. (Right) The ratio of phospho-KIF3A to non-phospho-KIF3A. The phosphorylation of KIF3A gradually increased in the neurons treated with TTX. **p < 0.01, ***p < 0.001, Dunnett's test.

(C) Site specificity of KIF3A phosphorylation by TTX stimulation. Cortical neurons (DIV 12) transfected with wild-type GFP–KIF3A WT or GFP–KIF3A AAA were treated with 0.01% DMSO (control) or TTX and then immunoblotted by Phos-tag WB with anti-GFP. GFP–KIF3A WT was phosphorylated under TTX treatment, whereas GFP–KIF3A AAA showed less phosphorylation.

(D) KIF3A AAA mutant reduced the effect of TTX. Hippocampal neurons coexpressed with RFP-KIF3A WT and N-cadherin-GFP showed N-cadherin accumulation under TTX stimulation, while neurons coexpressed with RFP-KIF3A AAA and N-cadherin-GFP showed little accumulation. Arrows indicate representative N-cadherin accumulation. Scale bar, 20 μm.

(E) Statics of N-cadherin accumulation (n = 5 neurons). Line chart, mean ± SD, ***p < 0.001, two-way repeated-measures ANOVA, Scheffé's post hoc test.

(F) Kymographs of N-cadherin–GFP transport in the neurons transfected with KIF3A WT or AAA. Neurons expressing KIF3A WT showed the same response to TTX treatment as shown in the Figure 6, while neurons expressing KIF3A AAA showed little N-cadherin transport before and after TTX treatment. Acquired live images were processed by the subtract function using the ImageJ image calculator, and the signals of N-cadherin movement were extracted. Scale bar, 20 μm.

(G) Statics of N-cadherin particles transported distally (n = 5 neurons). Histograms, mean ± SD, **p < 0.01, t test.

cargo-binding site produced higher cargo-binding affinity and facilitated N-cadherin transport (Figure 3) and that treatment with TTX enhanced the affinity and transport in vivo (Figure 6). Therefore, we analyzed the phosphorylation of KIF3A under chronic inactivation with TTX. Indeed, TTX treatment increased the proportion of phosphorylated KIF3A, but the total levels of both KIF3A and KAP3 proteins remained unchanged. Considering that the total levels of N-cadherin increased in both immunoblotting and time-lapse imaging analyses, the phosphorylation of KIF3A facilitated the transport of newly synthesized N-cadherin into spines in response to the TTX treatment (Figures 7A and 7B).

To confirm that site-specific phosphorylation of the KIF3A C terminus is induced downstream of chronic inactivation, cortical neurons transfected with GFP–KIF3A WT or the unphosphorylatable GFP–KIF3A AAA mutant were treated with or without bath application of TTX. Treated neurons were analyzed by Phos-tag WB. GFP–KIF3A WT was phosphorylated in the presence of TTX, whereas GFP–KIF3A AAA showed a band shift with lower phosphorylation (Figure 7C). These data confirmed that S689/T694/S698 of the KIF3A C terminus were phosphorylated downstream of chronic neuronal network inactivity produced by TTX. To confirm the site-specific contribution of KIF3A phosphorylation under chronic inactivation, we next observed N-cadherin transport in hippocampal neurons expressing KIF3A WT or AAA under TTX application. N-cadherin accumulation with TTX treatment was not induced in the neurons expressing KIF3A AAA
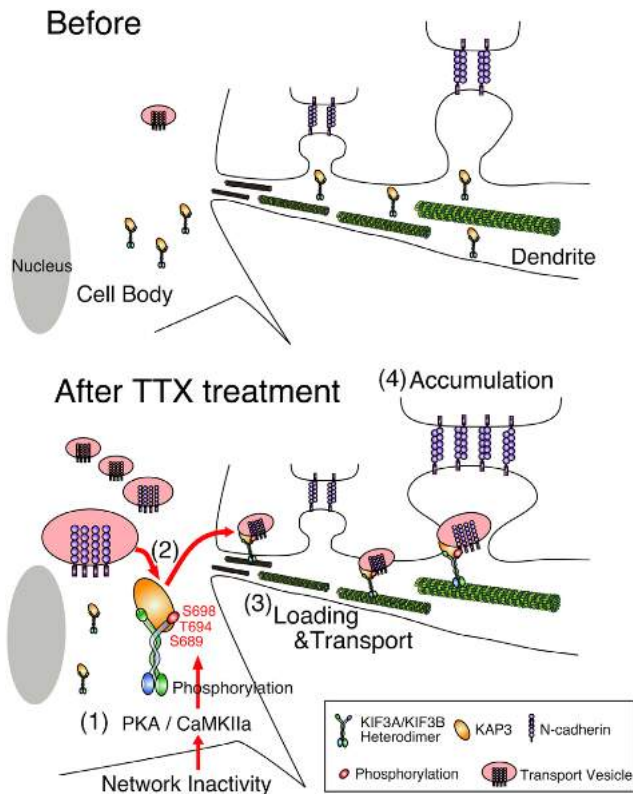
Figure 8. Model of Enhanced N-Cadherin Binding and Transport via KIF3A Phosphorylation in Homeostatic Synaptic Plasticity
(1) Chronic network inactivity triggers phosphorylation of S689/T694/S698 of KIF3A in the cargo-binding site. (2) This phosphorylation increases the affinity of the KIF3A C terminus with its cargo, N-cadherin, and (3) facilitates N-cadherin loading and transport via phosphorylated KIF3 under the control of PKA/CaMKIIa signaling pathways. (4) Enhanced N-cadherin transport via KIF3 induces N-cadherin accumulation into spines, resulting in synaptic enlargement.

(Figures 7D and 7E). In these neurons, N-cadherin transport was hardly observed before or after TTX application (Figures 7F and 7G). These results indicate that KIF3A AAA could not gain enough affinity to bind with N-cadherin because of specific unphosphorylatable mutations; thus, KIF3A AAA could not transport N-cadherin to spines. These mutation analyses in vivo confirmed that the specific phosphorylation of the KIF3A C terminus is critical for N-cadherin transport and accumulation in spines under chronic inactivation.

DISCUSSION

In this study, we investigated the activity-dependent cargo-loading mechanism in which phosphorylation of the KIF3A C terminus upregulates N-cadherin loading and transport. We identified key protein kinases of and phosphorylation sites on KIF3A that are responsible for cargo-loading activity and for the facilitation of N-cadherin transport, respectively, in an activity-dependent manner. We identified three critical sites, S689, T694, and S698, in the C-terminal cargo-binding site of KIF3A that were phosphorylated by PKA and CaMKIIa. Mutation ana-

lyses revealed that phosphorylation enhanced N-cadherin loading and transport, resulting in spine enlargement. Moreover, when neuronal activity was chronically suppressed by TTX, the phosphorylation levels of KIF3A were elevated. Simultaneously, the transport of N-cadherin was enhanced, thus resulting in global spine enlargement.

Taking all of these results together, we hereby propose a model for the mechanism of activity-dependent cargo loading: the phosphorylation of the KIF3A C terminus upregulates N-cadherin loading and transport (Figure 8). Before C-terminal phosphorylation, KIF3 is free from its cargo, N-cadherin. Once network inactivity is induced by TTX treatment, PKA/CaMKIIa phosphorylates S689, T694, and S698 in the KIF3A C-terminal cargo-binding site. This phosphorylation enhances the affinity between KIF3A and N-cadherin to facilitate N-cadherin loading, which induces N-cadherin transport and accumulation at spines; this activity plays a central role in homeostatic synaptic plasticity (Figure 8).

Activity-Dependent N-Cadherin Transport in Hebbian and Homeostatic Plasticity
In this study, we show that the phosphorylation of KIF3A increased the affinity between KIF3A and N-cadherin, enhanced the efficiency of N-cadherin loading and transport, and thus caused morphological changes to spine heads. Our findings are consistent with previous studies showing that disruption of N-cadherin increases immature filopodia-like protrusions and decreases postsynaptic protein accumulation (Okamura et al., 2004; Togashi et al., 2002). Furthermore, these findings are consistent with a previous report that activity-dependent N-cadherin accumulation alters spine morphology in Hebbian plasticity (Mendez et al., 2010). Note that Hebbian and homeostatic plasticity show some important differences in their molecular mechanisms, although these types of plasticity also share substantial overlap (Diering et al., 2014), including N-cadherin localization. Thus, our model can explain the mechanism of these previously reported phenomena in Hebbian and homeostatic plasticity.

PKA Is a Primary Kinase that Phosphorylates S689 in KIF3A
In our study, PKA preferentially phosphorylated S689, and CaMKIIa phosphorylated T694 and S698; all of these modifications enhanced the affinity between cargo and kinesin (individual data not shown). Moreover, not only PKA but also PKCα and RSK phosphorylated S689 in vitro. Loading cargo is a critical step in the transport process, and PKA functions as a primary kinase for this event; however, other kinases may support the function of PKA. Additional phosphorylation at T694 and S698 by CaMKIIa may also sustain or support the primary phosphorylation at S689. Some reports have indicated that CaMKII is primarily important for inducing cargo transport. This possibility should be carefully examined in the future (Phang et al., 2014).

Other Relevant Kinases
In this study, we identified phosphorylation sites and their responsible kinases using comprehensive approaches. Based on the sequence coverage (61%; Figure S1A), several possible phosphorylation sites may remain unidentified. In fact, kinases

other than PKA and CaMKIIa phosphorylated KIF3A in vitro (Figure 2A). Unphosphorylatable AAA mutants diminished the phosphorylation by CaMKII, whereas at least one additional site was phosphorylated by PKA (Figure 2C). Interestingly, kinase inhibitors did not affect the phosphorylation level in unstimulated neurons (Figure 2C). Moreover, thapsigargin treatment, which activates not only CaMKII but also PKC, induced more phosphorylation than expected (Figures 2D and 2E). Immunoblotting data (Figure 7C) also suggested the existence of additional phosphorylation sites under TTX treatment. Additional phosphorylation of KIF3 in response to calcium signaling cascades and chronic inactivation under various conditions will be an interesting subject for future research.

Phosphorylation of the Kinesin-2 C Terminus Affects Cargo-Binding Activity

The C-terminal cargo-binding site of KIF3A contains many alkaline amino acids (for example, Arg and Lys). The phosphorylation of this region could change the electrical charge to acidic, thereby influencing the interaction between KIF3 and cargoes. After loading a vesicle containing N-cadherin, KIF3 transports the cargo along the MTs. Activated PKA is reported to bind to the MT surface via MAP2 (Harada et al., 2002) and may sustain KIF3A phosphorylation to prevent KIF3A from releasing its cargo at inappropriate locations.

KIF3A and KIF17 both belong to the kinesin-2 family. Previous studies showed that phosphorylation of KIF17 by CaMKII released its cargo, GluN2B (Guillaud et al., 2008; Yin et al., 2012). By contrast, we demonstrate that phosphorylation of KIF3A by PKA/CaMKIIa increased its affinity with cargo. We speculate that CaMKII may contribute to specific cargo recognition and sorting that is dependent on its specific KIF under a specific signaling cascade. Indeed, these phosphorylation sites by CaMKII lie in C-terminal cargo-binding sites of KIF3A and KIF17. In contrast, CaMKII is ubiquitously distributed in cells. The spatial regulation of where these KIFs are phosphorylated by CaMKII will be an important subject in future studies to reveal all processes of cargo transport.

N-cadherin is reported to be transported via KIF5 (Heisler et al., 2014), and the transport of syntaxin via KIF5 is reported to be regulated by phosphorylation of its adaptor protein (Chua et al., 2012; Heisler et al., 2014). Our previous report showed that KIF5 knockout fibroblasts did not alter the distribution of N-cadherin (Teng et al., 2005); therefore, KIF3A is a primary transporter of N-cadherin and cooperates with other KIFs in each context. The effect of KIF3A phosphorylation on KIF5 activity is also particularly interesting.

Phosphorylation of the KIF3 C Terminus Has No Direct Effect on Its Motor Activity

In vitro experiment showed that phosphorylation itself did not directly affect the motor activity (Figures 3C and 3D). This result is consistent with the observation in vivo using overexpressed full-length KIF3A AAA/EEE mutants: both mutants could reach the growth cone in axons and the tips of dendritic shafts (Figure 4C). However, induced cargo binding may release the autoinhibition by another region at the C terminus. Thus, phosphorylation of KIF3 may indirectly affect its motor activity.

Tuned Mechanism to Sustain Proper Unloading and Transport

During TTX stimulation, we observed increased N-cadherin transport in both distal and proximal directions. The numbers of "stop" and "reverse" movements during N-cadherin transport also increased in both directions (Figure 6D). Interestingly, TTX treatment slightly decreased the velocity of N-cadherin transport (Figure 6E). We speculate that a local tuned mechanism may contribute to infallible cargo unloading at the proper destination. Further precise analyses of other phosphorylation sites or distinct mechanisms that directly control the motor activity are needed.

Temporal Regulation of N-Cadherin Expression and Transport during Homeostatic Synaptic Plasticity

Over the past decade, prolonged treatment with TTX has been shown to increase synaptic strength. However, the detailed mechanisms remain controversial because several sequential steps may be included in this process. In the present study, the amount of N-cadherin was initially reduced for 1 hr after TTX stimulation but recovered beyond the prestimulation level over the next several hours (Figure 7A). In the short term, TTX stimulation immediately reduces the protease resistance of N-cadherin and the association between N-cadherin and β-catenin (Murase et al., 2002; Tanaka et al., 2000). N-cadherin instability also reduces the surface expression level of AMPARs and the number of miniature excitatory synaptic events (Vitureira et al., 2012), thus inhibiting both action potentials and miniature excitatory synaptic events and resulting in the activation of dendritic protein synthesis (Sutton et al., 2004). Over the long term, newly synthesized N-cadherin would be transported into spines; consequently, postsynaptic strength would be increased, as described in this study. We observed that KIF3A phosphorylation was elevated in the same phase as the increase in N-cadherin expression (Figure 7B). Thus, temporal regulation likely contributes to tuning the delivery mechanism in both homeostatic synaptic plasticity and L-LTP. Furthermore, the combination of Hebbian and homeostatic plasticity seems to sustain proper network activities in higher brain functions such as memory consolidation during sleep. Validation of KIF3A phosphorylation and N-cadherin transport under memory consolidation would be challenging future work.

In conclusion, we have shown that chronic network inactivity induced phosphorylation of the KIF3A cargo-binding site and facilitated the loading and transport of N-cadherin via the PKA/CaMKIIa signaling pathways. These activities caused the accumulation of N-cadherin at spines, which is a key factor in homeostatic synaptic plasticity. Thus, this study shows that KIF3A has an important role in regulating homeostatic synaptic plasticity through phosphorylation and presents a model of the mechanism of activity-dependent cargo loading.

EXPERIMENTAL PROCEDURES

Detailed methods are available in the Supplemental Experimental Procedures.

KIF3A Constructs

Full-length KIF3A was ligated into multiple cloning sites of the pEGFP-N1 plasmid (Clontech) to create GFP–KIF3A. KIF3A point mutation constructs

S689A/T694A/S698A and S689E/T694E/S698E were produced by PCR. Details are provided in Figure S2.

KIF3A motor (M1-S381)-GFP-His, which was ligated into the pET21b plasmid (Novagen), was bacterially expressed and purified by IMAC and size exclusion chromatography.

Antibodies, Brain Lysate Fractionation, and Endogenous Protein Immunoprecipitation

Antibodies and fractions of brain lysate were prepared as described in the Supplemental Experimental Procedures. Precleared proper fractions were incubated with anti-KIF3A/KAP3 and anti-N-cadherin antibodies. These protein complexes were captured with magnetic μMACS Protein G MicroBeads (Miltenyi Biotec) and eluted using magnetic MACS M Columns (Miltenyi Biotec).

Phos-Tag SDS-PAGE and Western Blot Analyses

Electrophoresis with 30 mM Zn^{2+} Phos-tag (Wako, Japan) (Kinoshita et al., 2006) in 6% or 7.5% acrylamide gels was performed, followed by CBB staining or WB analysis. CBB staining was performed in a manner identical to that for normal SDS-PAGE. For WB analysis, the divalent cations were removed after electrophoresis by incubation with transfer buffer containing 5 mM EDTA. The gel contents were transferred to polyvinyl difluoride membrane using standard methods.

GST Pull-Down

GST–KIF3A CT wild-type, S689A/T694A/S698A, and S689E/T694E/S698E, which were ligated into the pGEX-6P-3 vector (GE Healthcare), were expressed in *E. coli*. The brain S2 fraction was precleared and applied to GST–KIF3A CT-bound affinity columns. The columns were washed extensively, followed by elution with 10 mM reduced glutathione.

MT Gliding Assays and ATPase Measurements

MT gliding assays were performed using a standard method as described previously (Carter and Cross, 2001). Purified KIF3A motor was immobilized in a glass chamber with penta-His antibody (QIAGEN). Taxol-stabilized TMR-labeled MTs were added to the chamber with purified KIF3A C-terminal WT or mutants (10 mM), GST-CBS WT/AAA/EEE (Figure S2). Time-lapse images were acquired using the ELYRA P.1 system (Carl Zeiss) at 27°C. To analyze ATPase activity, 1 nmol KIF3A motor was incubated with polymerized MTs (1 nmol tubulin dimer) and 100 nmol ATP (Roche) for 30 min at 27°C in the presence of 1 mM KIF3A C-terminal mutants. Released ADP and bound ATP were separated by anion exchange chromatography on an AKTA system (GE) and directly quantified from the peak area of each chromatogram.

Culture, Transfection, and Chemicals

Hippocampal and cortical cells were obtained from mouse brains on embryonic day 17. Plasmids were transfected using a High-Efficiency Ca^{2+} Phosphate Transfection Kit (BD Bioscience) as reported previously (Jiang and Chen, 2006). For phosphorylation analyses, cells were treated with forskolin (10 μM), KT5720 (1 μM), KN-93 (1 μM; Calbiochem), thapsigargin (1 μM), or TTX (1 μM; Wako).

Fixation, Microscopy, and Imaging Analysis

Neurons were fixed in 4% paraformaldehyde and 4% sucrose in PBS. Images of fixed neurons were acquired with a LSM710 or LSM780 confocal microscope system (Carl Zeiss). Pyramidal-like neurons were chosen randomly for quantification. For colocalization assays, 1 mM adenylyl imidodiphosphate (AMP-PNP) and 0.01% saponin were added to the medium before fixation. Immunostaining was performed as described in the Supplemental Experimental Procedures. Time-lapse imaging (Figure 5) was performed with a LSM 5 LIVE system (Carl Zeiss). Time-lapse imaging analysis under TTX stimulation (Figures 6 and 7) was conducted using an inverted fluorescent microscope (Axio Observer.Z1, ZEISS) equipped with a spinning-disk confocal unit (CSU-W1, Yokogawa). All data were analyzed using ImageJ software (Wayne Rasband) with the Particle Tracker plug-in (MOSAIC group, ETH Zurich) and Kymograph plug-in (Rietdorf and Seitz).

Protein Identification and Phosphopeptide Quantitation

Protein samples were reduced, alkylated, and digested. For protein identification, peptides were desalted and spotted on sample plates with a CHCA matrix. The MS/MS data were obtained using an ABI 4700 MALDI-TOF mass spectrometer (AB Sciex). For phosphopeptide quantitation, the digested peptides were labeled with TMT Reagents (Thermo Scientific) and analyzed on an LTQ-FTMS mass spectrometer (Thermo) interfaced with a nanoelectrospray ion source. All data were searched against the mouse NCBI database and the mouse Swiss-Prot database using SEQUEST and MASCOT (Matrix Science).

Statistical Analysis

Immunoblots were analyzed by t test. Cumulative frequency data were analyzed by the Kolmogorov-Smirnov test. For comparizations between groups, one-way ANOVA with a Scheffé's post hoc test was used, and two-way repeated-measures ANOVA with a Bonferroni's post hoc test was used if several time points existed.

SUPPLEMENTAL INFORMATION

Supplemental Information includes four figures and Supplemental Experimental Procedures and can be found with this article at http://dx.doi.org/10.1016/j.neuron.2015.08.008.

REFERENCES

Banke, T.G., Bowie, D., Lee, H., Huganir, R.L., Schousboe, A., and Traynelis, S.F. (2000). Control of GluR1 AMPA receptor function by cAMP-dependent protein kinase. J. Neurosci. 20, 89–102.

Bemben, M.A., Shipman, S.L., Hirai, T., Herring, B.E., Li, Y., Badger, J.D., 2nd, Nicoll, R.A., Diamond, J.S., and Roche, K.W. (2014). CaMKII phosphorylation of neuroligin-1 regulates excitatory synapses. Nat. Neurosci. 17, 56–64.

Benson, D.L., and Tanaka, H. (1998). N-cadherin redistribution during synaptogenesis in hippocampal neurons. J. Neurosci. 18, 6892–6904.

Bozdagi, O., Shan, W., Tanaka, H., Benson, D.L., and Huntley, G.W. (2000). Increasing numbers of synaptic puncta during late-phase LTP: N-cadherin is synthesized, recruited to synaptic sites, and required for potentiation. Neuron 28, 245–259.

Brigidi, G.S., and Bamji, S.X. (2011). Cadherin-catenin adhesion complexes at the synapse. Curr. Opin. Neurobiol. 21, 208–214.

Carter, N., and Cross, R. (2001). An improved microscope for bead and surface-based motility assays. Methods Mol. Biol. *164*, 73–89.

Chua, J.J., Butkevich, E., Worseck, J.M., Kittelmann, M., Grønborg, M., Behrmann, E., Stelzl, U., Pavlos, N.J., Lalowski, M.M., Eimer, S., et al. (2012). Phosphorylation-regulated axonal dependent transport of syntaxin 1 is mediated by a Kinesin-1 adapter. Proc. Natl. Acad. Sci. USA *109*, 5862–5867.

Diering, G.H., Gustina, A.S., and Huganir, R.L. (2014). PKA-GluA1 coupling via AKAP5 controls AMPA receptor phosphorylation and cell-surface targeting during bidirectional homeostatic plasticity. Neuron *84*, 790–805.

Dietrich, K.A., Sindelar, C.V., Brewer, P.D., Downing, K.H., Cremo, C.R., and Rice, S.E. (2008). The kinesin-1 motor protein is regulated by a direct interaction of its head and tail. Proc. Natl. Acad. Sci. USA *105*, 8938–8943.

Esteban, J.A., Shi, S.-H., Wilson, C., Nuriya, M., Huganir, R.L., and Malinow, R. (2003). PKA phosphorylation of AMPA receptor subunits controls synaptic trafficking underlying plasticity. Nat. Neurosci. *6*, 136–143.

Frey, U., Huang, Y.Y., and Kandel, E.R. (1993). Effects of cAMP simulate a late stage of LTP in hippocampal CA1 neurons. Science *260*, 1661–1664.

Gu, Y., and Gu, C. (2010). Dynamics of Kv1 channel transport in axons. PLoS ONE *5*, e11931.

Gu, C., Zhou, W., Puthenveedu, M.A., Xu, M., Jan, Y.N., and Jan, L.Y. (2006). The microtubule plus-end tracking protein EB1 is required for Kv1 voltage-gated K+ channel axonal targeting. Neuron *52*, 803–816.

Guillaud, L., Wong, R., and Hirokawa, N. (2008). Disruption of KIF17-Mint1 interaction by CaMKII-dependent phosphorylation: a molecular model of kinesin-cargo release. Nat. Cell Biol. *10*, 19–29.

Guo, X., Macleod, G.T., Wellington, A., Hu, F., Panchumarthi, S., Schoenfield, M., Marin, L., Charlton, M.P., Atwood, H.L., and Zinsmaier, K.E. (2005). The GTPase dMiro is required for axonal transport of mitochondria to Drosophila synapses. Neuron *47*, 379–393.

Harada, A., Teng, J., Takei, Y., Oguchi, K., and Hirokawa, N. (2002). MAP2 is required for dendrite elongation, PKA anchoring in dendrites, and proper PKA signal transduction. J. Cell Biol. *158*, 541–549.

Heisler, F.F., Lee, H.K., Gromova, K.V., Pechmann, Y., Schurek, B., Ruschkies, L., Schroeder, M., Schweizer, M., and Kneussel, M. (2014). GRIP1 interlinks N-cadherin and AMPA receptors at vesicles to promote combined cargo transport into dendrites. Proc. Natl. Acad. Sci. USA *111*, 5030–5035.

Hell, J.W. (2014). CaMKII: claiming center stage in postsynaptic function and organization. Neuron *81*, 249–265.

Hill, E., Clarke, M., and Barr, F.A. (2000). The Rab6-binding kinesin, Rab6-KIFL, is required for cytokinesis. EMBO J. *19*, 5711–5719.

Hirokawa, N. (1998). Kinesin and dynein superfamily proteins and the mechanism of organelle transport. Science *279*, 519–526.

Hirokawa, N., Noda, Y., Tanaka, Y., and Niwa, S. (2009a). Kinesin superfamily motor proteins and intracellular transport. Nat. Rev. Mol. Cell Biol. *10*, 682–696.

Hirokawa, N., Tanaka, Y., and Okada, Y. (2009b). Left-right determination: involvement of molecular motor KIF3, cilia, and nodal flow. Cold Spring Harb. Perspect. Biol. *1*, a000802.

Hirokawa, N., Niwa, S., and Tanaka, Y. (2010). Molecular motors in neurons: transport mechanisms and roles in brain function, development, and disease. Neuron *68*, 610–638.

Hoerndli, F.J., Wang, R., Mellem, J.E., Kallarackal, A., Brockie, P.J., Thacker, C., Madsen, D.M., and Maricq, A.V. (2015). Neuronal activity and CaMKII regulate kinesin-mediated transport of synaptic AMPARs. Neuron *86*, 457–474.

Imanishi, M., Endres, N.F., Gennerich, A., and Vale, R.D. (2006). Autoinhibition regulates the motility of the *C. elegans* intraflagellar transport motor OSM-3. J. Cell Biol. *174*, 931–937.

Jiang, M., and Chen, G. (2006). High Ca2+-phosphate transfection efficiency in low-density neuronal cultures. Nat. Protoc. *1*, 695–700.

Kinoshita, E., Kinoshita-Kikuta, E., Takiyama, K., and Koike, T. (2006). Phosphate-binding tag, a new tool to visualize phosphorylated proteins. Mol. Cell. Proteomics *5*, 749–757.

Kondo, S., Sato-Yoshitake, R., Noda, Y., Aizawa, H., Nakata, T., Matsuura, Y., and Hirokawa, N. (1994). KIF3A is a new microtubule-based anterograde motor in the nerve axon. J. Cell Biol. *125*, 1095–1107.

Lee, K.J., Queenan, B.N., Rozeboom, A.M., Bellmore, R., Lim, S.T., Vicini, S., and Pak, D.T. (2013). Mossy fiber-CA3 synapses mediate homeostatic plasticity in mature hippocampal neurons. Neuron *77*, 99–114.

Malenka, R.C., and Bear, M.F. (2004). LTP and LTD: an embarrassment of riches. Neuron *44*, 5–21.

Mendez, P., De Roo, M., Poglia, L., Klauser, P., and Muller, D. (2010). N-cadherin mediates plasticity-induced long-term spine stabilization. J. Cell Biol. *189*, 589–600.

Murase, S., Mosser, E., and Schuman, E.M. (2002). Depolarization drives β-catenin into neuronal spines promoting changes in synaptic structure and function. Neuron *35*, 91–105.

Nishimura, T., Kato, K., Yamaguchi, T., Fukata, Y., Ohno, S., and Kaibuchi, K. (2004). Role of the PAR-3-KIF3 complex in the establishment of neuronal polarity. Nat. Cell Biol. *6*, 328–334.

Niwa, S., Tanaka, Y., and Hirokawa, N. (2008). KIF1Bbeta- and KIF1A-mediated axonal transport of presynaptic regulator Rab3 occurs in a GTP-dependent manner through DENN/MADD. Nat. Cell Biol. *10*, 1269–1279.

Okamura, K., Tanaka, H., Yagita, Y., Saeki, Y., Taguchi, A., Hiraoka, Y., Zeng, L.H., Colman, D.R., and Miki, N. (2004). Cadherin activity is required for activity-induced spine remodeling. J. Cell Biol. *167*, 961–972.

Okuda, T., Yu, L.M., Cingolani, L.A., Kemler, R., and Goda, Y. (2007). beta-Catenin regulates excitatory postsynaptic strength at hippocampal synapses. Proc. Natl. Acad. Sci. USA *104*, 13479–13484.

Opazo, P., Labrecque, S., Tigaret, C.M., Frouin, A., Wiseman, P.W., De Koninck, P., and Choquet, D. (2010). CaMKII triggers the diffusional trapping of surface AMPARs through phosphorylation of stargazin. Neuron *67*, 239–252.

Phang, H.Q., Hoon, J.L., Lai, S.K., Zeng, Y., Chiam, K.H., Li, H.Y., and Koh, C.G. (2014). POPX2 phosphatase regulates the KIF3 kinesin motor complex. J. Cell Sci. *127*, 727–739.

Roche, K.W., O'Brien, R.J., Mammen, A.L., Bernhardt, J., and Huganir, R.L. (1996). Characterization of multiple phosphorylation sites on the AMPA receptor GluR1 subunit. Neuron *16*, 1179–1188.

Stowers, R.S., Megeath, L.J., Górska-Andrzejak, J., Meinertzhagen, I.A., and Schwarz, T.L. (2002). Axonal transport of mitochondria to synapses depends on milton, a novel *Drosophila* protein. Neuron *36*, 1063–1077.

Sutton, M.A., Wall, N.R., Aakalu, G.N., and Schuman, E.M. (2004). Regulation of dendritic protein synthesis by miniature synaptic events. Science *304*, 1979–1983.

Takeichi, M. (2014). Dynamic contacts: rearranging adherens junctions to drive epithelial remodelling. Nat. Rev. Mol. Cell Biol. *15*, 397–410.

Tanaka, H., Shan, W., Phillips, G.R., Arndt, K., Bozdagi, O., Shapiro, L., Huntley, G.W., Benson, D.L., and Colman, D.R. (2000). Molecular modification of N-cadherin in response to synaptic activity. Neuron *25*, 93–107.

Teng, J., Rai, T., Tanaka, Y., Takei, Y., Nakata, T., Hirasawa, M., Kulkarni, A.B., and Hirokawa, N. (2005). The KIF3 motor transports N-cadherin and organizes the developing neuroepithelium. Nat. Cell Biol. *7*, 474–482.

Togashi, H., Abe, K., Mizoguchi, A., Takaoka, K., Chisaka, O., and Takeichi, M. (2002). Cadherin regulates dendritic spine morphogenesis. Neuron *35*, 77–89.

Tononi, G., and Cirelli, C. (2014). Sleep and the price of plasticity: from synaptic and cellular homeostasis to memory consolidation and integration. Neuron *81*, 12–34.

Turrigiano, G.G. (2008). The self-tuning neuron: synaptic scaling of excitatory synapses. Cell *135*, 422–435.

Vitureira, N., and Goda, Y. (2013). Cell biology in neuroscience: the interplay between Hebbian and homeostatic synaptic plasticity. J. Cell Biol. *203*, 175–186.

Vitureira, N., Letellier, M., White, I.J., and Goda, Y. (2012). Differential control of presynaptic efficacy by postsynaptic N-cadherin and β-catenin. Nat. Neurosci. *15*, 81–89.

Yamazaki, H., Nakata, T., Okada, Y., and Hirokawa, N. (1996). Cloning and characterization of KAP3: a novel kinesin superfamily-associated protein of KIF3A/3B. Proc. Natl. Acad. Sci. USA *93*, 8443–8448.

Yin, X., Feng, X., Takei, Y., and Hirokawa, N. (2012). Regulation of NMDA receptor transport: a KIF17-cargo binding/releasing underlies synaptic plasticity and memory *in vivo*. J. Neurosci. *32*, 5486–5499.